Table 2 Critical combination of the load parameters λ_p and λ_q of a spring-hinged cantilever column

γ	$\lambda_{p\,\mathrm{cr}}$	$\lambda_{q\,\mathrm{cr}}$	$\alpha(\lambda_q/\lambda_{q\,\mathrm{cr}})$	λ_p	$\beta(\lambda_p/\lambda_{p\,\mathrm{cr}})$	$\alpha+\beta$
1.0	0.7405	1.665	0.2	0.5942	0.8025	1.002
1.0	0.7405	1.665	0.4	0.4471	0.6038	1.004
1.0	0.7405	1.665	0.6	0.2990	0.4038	1.004
1.0	0.7405	1.665	0.8	0.1500	0.2025	1.002
10	2.054	5.957	0.2	1.655	0.8058	1.006
10	2.054	5.957	0.4	1.250	0.6087	1.009
10	2.054	5.957	0.6	0.8394	0.4087	1.009
10	2.054	5.957	0.8	0.4227	0.2058	1.006
100	2.437	7.657	0.2	1.9640	0.8060	1.006
100	2.437	7.657	0.4	1.4840	0.6090	1.009
100	2.437	7.657	0.6	0.9966	0.4090	1.009
100	2.437	7.657	0.8	0.5020	0.2060	1.006

very well with those obtained from the FEM for all values of the rotational spring stiffness parameter γ varying from 1 to 10^{11} ($\rightarrow \infty$), the maximum error being around 0.7% for the value of $\gamma = 10^{11}$. Also note that the stability parameters obtained by the FEM are in excellent agreement with those given by Timoshenko and Gere.[3]

For the combined loading, the combination values of λ_p and λ_q for which the spring-hinged column buckles are given in Table 2, for $\gamma = 1$, 10, and 100. Note that, for the combined loading, the sum of $\lambda_p/\lambda_{p\,\mathrm{cr}}$ and $\lambda_q/\lambda_{q\,\mathrm{cr}}$ is almost equal to 1.0, with the nonzero term being in the fourth significant figure. The authors have verified this for all of the values of γ considered in Table 1. It is believed that this small difference from unity in the fourth significant figure is due to the numerical approximation involved in the present computations. Hence, we can generalize this observation as follows.

Irrespective of the rotational spring stiffness, for a spring-hinged cantilever column subjected to combined axial concentrated end load and uniformly distributed load, we can take

$$\lambda_p/\lambda_{p\,\mathrm{cr}} + \lambda_q/\lambda_{q\,\mathrm{cr}} = 1 \tag{9}$$

effectively for design purposes. Equation (9) is valid for any mutually independent and simultaneously acting axial compressive concentrated load and uniformaly distributed axial compressive load.

Conclusions

The stability behavior of a spring-hinged cantilever column subjected to mutually independent and simultaneously acting end-compressive and uniformly distributed axial loads is studied in this Note by use of the Rayleigh–Ritz method. The novelty of this study is choosing proper admissible functions to satisfy the spring-hinged boundary condition. Closed-form expressions are obtained for the combination of loads for which the column buckles. The method is validated by comparing the present results with those obtained by the FEM for the cases of independent loads. Finally, a simple, elegant design formula for the combined loading is given based on the numerical results obtained. It is expected that it will be useful for aerospace engineers in particular, and structural engineers, in general.

References

[1]Zienkiewicz, O. C., *The Finite Element Method*, McGraw–Hill Ltd., London, 1977.

[2]Elishakoff, I., "Apparently First Closed-Form Solution for Frequency of Beam with Rotational Spring," *AIAA Journal*, Vol. 39, No. 1, 2001, pp. 183–186.

[3]Timoshenko, S. P., and Gere, J. M., *Theory of Elastic Stability*, McGraw–Hill, New York, 1961, pp. 89–103.

A. M. Waas
Associate Editor

Vortical Substructures in the Shear Layers Forming Leading-Edge Vortices

Anthony M. Mitchell*
U.S. Air Force Academy, Colorado Springs, Colorado 80840-6222
and
Pascal Molton†
ONERA, 92190 Meudon, France

Introduction

SUBSTANTIAL theoretical, experimental, and computational research has focused on the characteristics of leading-edge vortices and vortex breakdown.[1–8] However, limited efforts have sought to understand the separating shear layers that roll up to form the leading-edge vortices. Various researchers have observed discrete vortical substructures in the shear layers, and the resulting data have taken on two contrasting descriptions: temporal substructures (rotating around the leading-edge vortex)[9–11] and spatially stationary substructures (spatially fixed around the periphery of the leading-edge vortex).[12–19] Additionally, many of these researchers have hypothesized about the type of instability that results in the formation of the vortical substructures. None of these hypotheses has been universally accepted or proven. The most popular hypothesis[9,11,13,14,17,18] proposes that the substructures develop in a manner similar to the Kelvin–Helmholtz[20] instability or that of a two-dimensional shear-layer instability described by Ho and Huerre.[21] Another hypothesis suggests that the substructures originate from transversal perturbations along the leading edge of the wing induced by the interaction between the separating shear layer and the secondary vortices.[10,19] Washburn and Visser[16] suggested the substructures are generated by nonviscous instabilities in the shear layer and that their formation is governed by transverse flow of the leading-edge vortices. Yet another hypothesis postulates that a longitudinal instability associated with the curvature of the separating shear layer is at the origin of the substructures.[17] Some experimentally based hypotheses indicate that the instabilities are generated by the presence of small-amplitude surface waves in the water tunnel[10] or are associated with vibrations in a wind tunnel.[14]

Recent advances in nonintrusive experimental measurement techniques have enabled more detailed analysis of the vortical flowfield and the separating shear layers forming the leading-edge vortices around a delta wing. Three-dimensional laser Doppler velocimetry (LDV) flowfield measurements were acquired in ONERA's 1.4×1.8 m subsonic wind tunnel around a sharp-edged delta wing model.[22–24] These novel results provide new insight into the phenomenon through precisely measured details of the characteristics and path of the vortical substructures around the leading-edge vortex core.

Model and Wind Tunnel

The delta wing model has a 70-deg sweep angle and root chord c of 950 mm. It has a wingspan of 691.5 mm at its trailing edge, is

Presented as Paper 2001-2424 at the 19th Applied Aerodynamics Conference, Anaheim, CA, 11–14 June 2001; received 21 June 2001; revision received 18 April 2002; accepted for publication 18 April 2002.

*Major, U.S. Air Force, and Assistant Professor, Department of Aeronautics, 2354 Fairchild Drive, Suite 6H39C. Senior Member AIAA.

†Research Engineer, Fundamental and Experimental Aerodynamics Department, 8 rue des Vertugadins.

20 mm thick, and is beveled on the windward side at an angle of 15 deg to form sharp leading edges. All of the data presented here were acquired in ONERA's 1.4×1.8 m subsonic wind tunnel (F2) at test conditions of $\alpha = 27$ deg and $U_\infty = 24$ m/s ($Re_c = 1.56 \times 10^6$). Because of the relative symmetry of the flowfield over the leeward surface of the delta wing, only the port-side flowfield was examined. Details of the model, the wind tunnel, and LDV system are specified in Refs. 23 and 24.

Accuracy and Experimental Error

In ONERA's F2 wind tunnel the relative freestream velocity $\Delta U_\infty / U_\infty$ is estimated to have an accuracy of $\pm 1\%$, whereas the mean intensity of turbulence is approximately 0.1%. The model was mounted on a sting with a horizontal support and flexible joint for adjusting the angle of attack, with an accuracy of ± 0.05 deg. The horizontal support was manipulated in height along a vertical column so as to maintain the model close to the center axis of the test section. The model was mounted in the test section with no yaw angle with respect to the freestream flow (estimated accuracy of ± 0.1 deg).[23,24] The LDV system installed in F2 utilizes two 15-W argon lasers as the sources of light in a forward scattering mode. The global accuracy of the LDV system is estimated to have a relative error $\Delta U / U$ of less than 1.5% assuming an absolute error of the angle between the velocity vector and a horizontal reference of 0.5 deg. Therefore, the estimated accuracy of the magnitude of the velocity is ± 1 m/s, and the direction of the velocity vector is ± 1 deg (Ref. 25).

Results

Four LDV planes perpendicular to the leeward surface of the wing at $X/c = 0.53$, 0.63, 0.74, and 0.84 were explored. These planes correspond to a region where the leading-edge vortex was well developed: a zone just upstream of the vortex breakdown location, a zone downstream of the vortex breakdown location, and finally a region further downstream where the flow was fully turbulent. Each perpendicular measurement mesh consists of approximately 1400 points located between $0.4 < Y/b < 1.1$ on the port side of the wing, evenly spaced at 5-mm intervals.

The results demonstrate a strong, jetlike, acceleration of the flow along the vortex core upstream of vortex breakdown ($X/c = 0.65$) with values of $U/U_\infty \geq 3.5$. There is an abrupt deceleration of the axial velocity component to a stagnation point (vortex breakdown location), which is followed by a zone of recirculation and a sizeable increase in the diameter of the vortex core. The postbreakdown region has a wake-like axial velocity profile. Components of vorticity are calculated from the measured mean velocity components using a central differencing scheme to evaluate the derivatives. Figure 1 represents the axial component of vorticity ($\Omega_x = \partial W/\partial y - \partial V/\partial z$) in each perpendicular plane. These traces reveal two highly rotational zones in the flowfield: 1) the vortex core with a highly negative vorticity; 2) regions of positive vorticity near the leading edge, along the suction surface of the wing, which represent the secondary vortex. Additionally, multiple substructures, rotating in the same direction as the vortex core, are clearly defined in the time-averaged data and confirm the observations of the existence of spatially stationary substructures. It is clear from the dissipation of the vorticity in the vortex core in Figs. 1c and 1d that vortex breakdown has occurred. However, the vortical substructures are still present in the flowfield around the vortex core.

Because of the large spacing interval between the perpendicular planes of data presented in Fig. 1, a second series of experiments was conducted to acquire data from 12 perpendicular planes over the

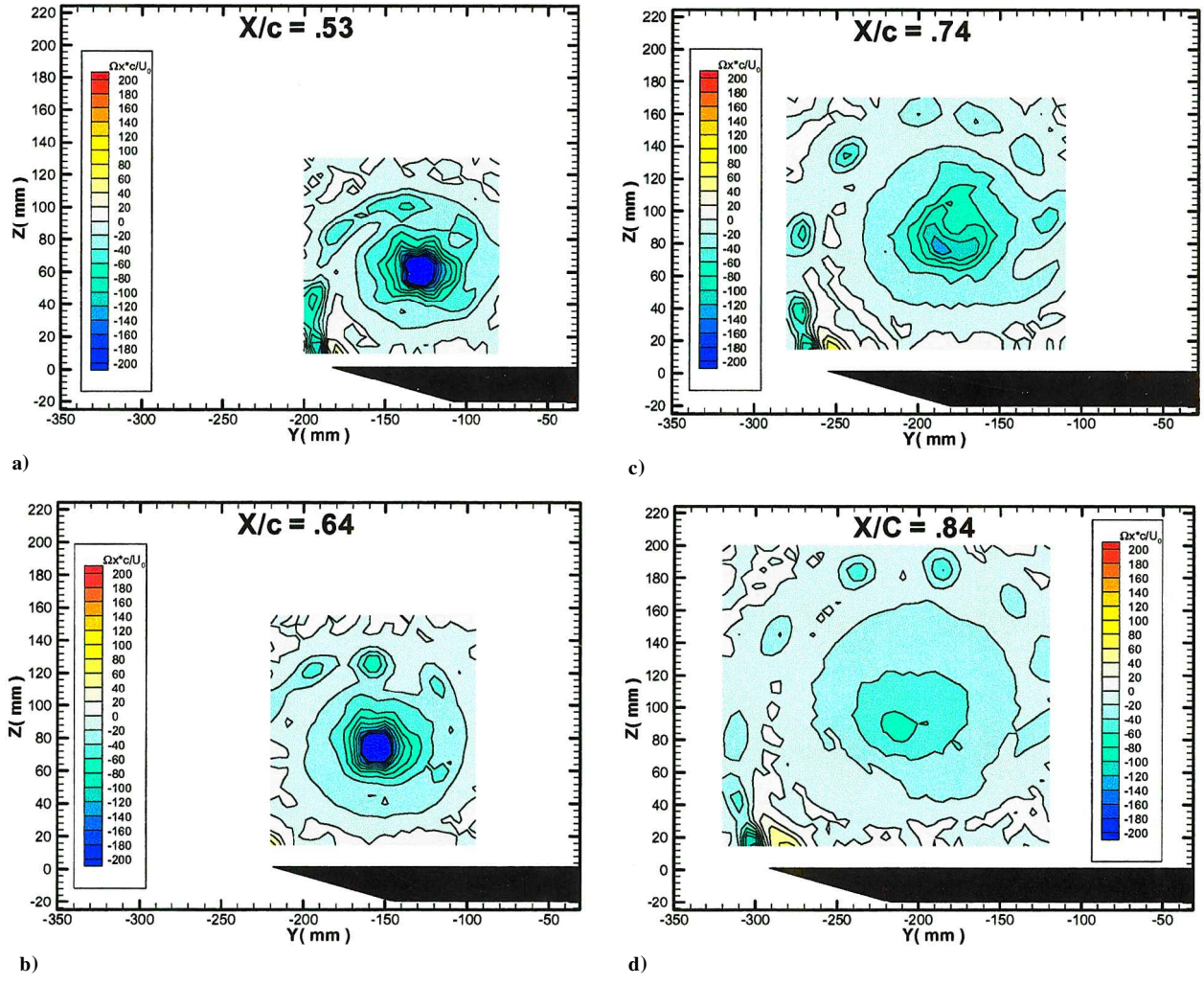

Fig. 1 LDV results showing the axial vorticity ($\Omega_x c/U_\infty$) at $\alpha = 27$ deg and $U_\infty = 24$ m/s: a) $X/c = 0.53$ (500 mm), b) $X/c = 0.64$ (600 mm), c) $X/c = 0.74$ (700 mm), and d) $X/c = 0.84$ (800 mm).

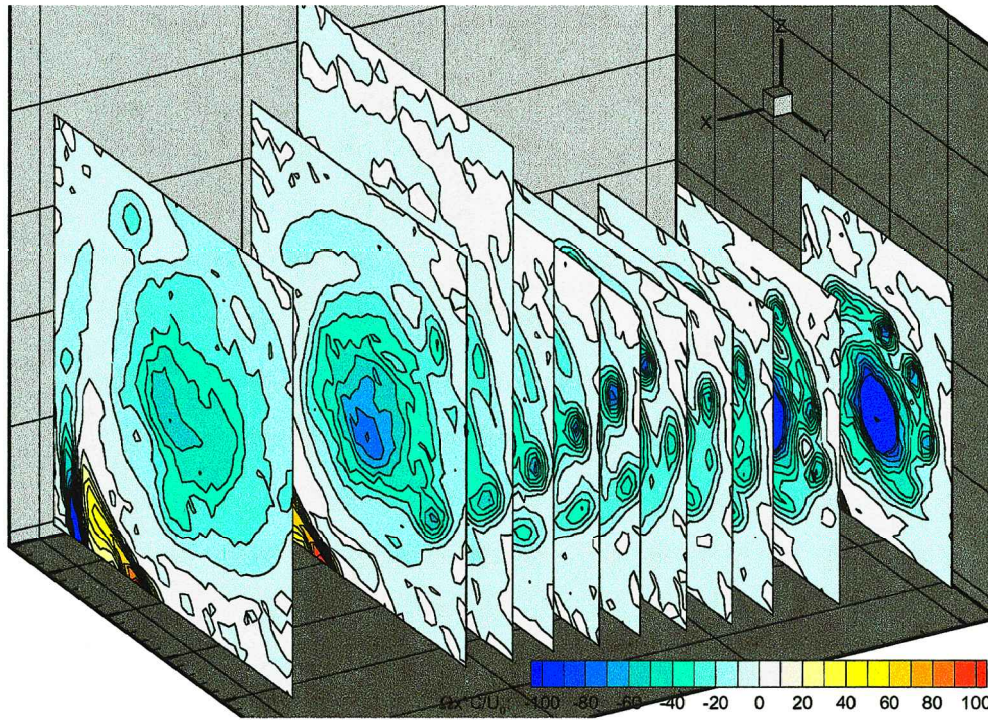

Fig. 2 Vortical substructures measured in different planes perpendicular to the leeward surface of the 70-deg delta wing at $\alpha = 27$ deg and $Re_c = 15.6 \times 10^6$ (freestream velocity from right to left).

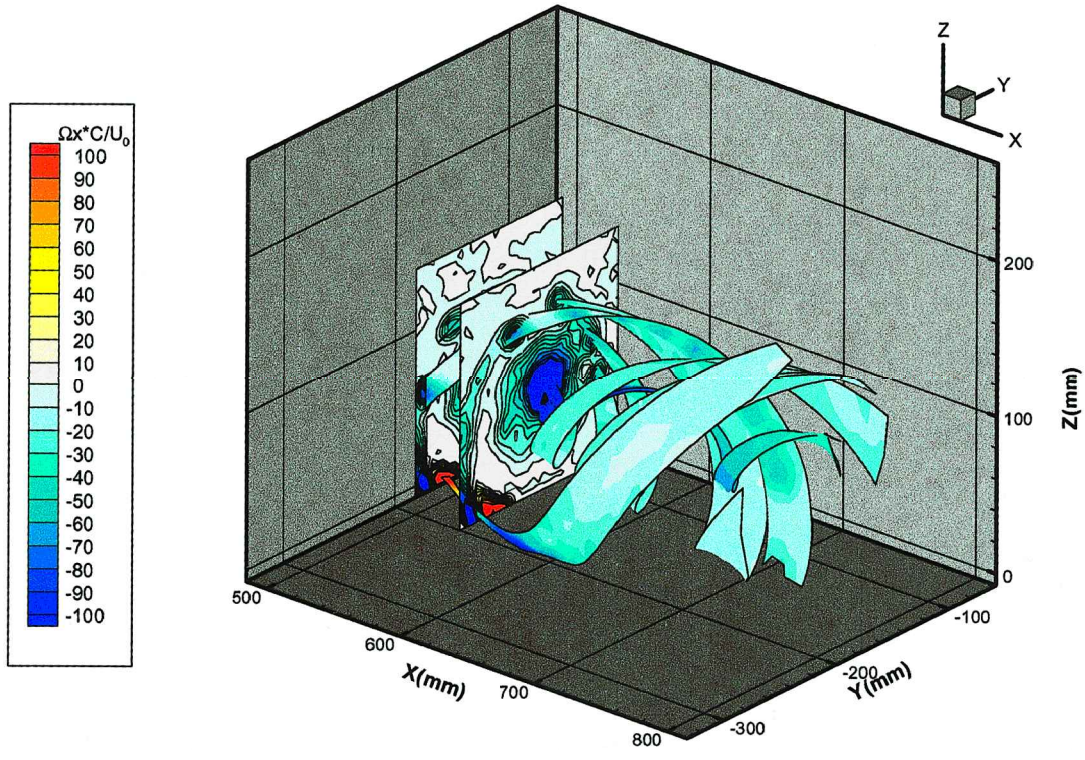

Fig. 3 Interpolated stream ribbons following the vortical substructures around the vortex core showing values of the axial vorticity ($\Omega_x c/U_\infty$) at $\alpha = 27$ deg and $Re_c = 1.56 \times 10^6$ (freestream velocity from left to right).

same region of the wing. These perpendicular planes were situated at $X/c = 0.53, 0.58, 0.61, 0.63, 0.65, 0.67, 0.69, 0.72, 0.74, 0.76$, and 0.84. The data were acquired using the same measurement meshes as the data shown in Fig. 1, although the delta wing model was rotated around its chord line by the addition of a wedge between the windward surface of the delta wing model and the sting. The effective incidence angle of the model with respect to the freestream velocity of the wind tunnel was maintained by simultaneously maneuvering the angles of the sting's elbow joints. This rotation of the model caused the time-averaged vortex breakdown location to shift upstream approximately 100 mm (10.5% of the chord). This was the only observed modification to the flowfield as a result of the model's rotation, and the results remained within the outliers of the observed instantaneous breakdown locations for both configurations. The new, more finely probed, volume of data constitutes an important database for interpolation across the entire flowfield.

The results shown in Fig. 2 demonstrate the evolution of the discrete substructures of vorticity around the vortex core. The substructures appear to roll around the vortex core as they evolve in the downstream direction. The magnitude of the axial component vorticity in each of the substructures is of the same order of magnitude as that measured in the vortex core. One also observes a decrease in the magnitude of the axial component of vorticity proportional to the increase in the longitudinal distance X/c. This trend indicates the presence of a local instability near the leading edge, which is generating the substructures. Therefore, it is proposed that the substructures are formed near the leading edge and are subsequently entrained downstream by both the axial velocity of the flow and the rotational velocity of the leading-edge vortex. The substructures follow a helical trajectory around the vortex core, and the spacing (frequency) between the substructures appears relatively constant, confirming the observations of Washburn and Visser.[16] Additionally, the substructures remain coherent even in the postbreakdown region of the flowfield.

Figure 3 illustrates the three-dimensional flowfield developing around the delta wing. This image was computed by interpolating the data between the various perpendicular planes of measurements. The first two planes, at $X/c = 0.53$ and 0.58, are shown. The rest of the data represents various stream ribbons, initiated at the center of the substructures in the first perpendicular planes, which pass through the centers of the subsequent substructures. The values indicated on the stream ribbons represent the axial component of vorticity. These stream ribbons represent the helical trajectory of the substructures around the vortex core with constant spacing. As observed in Fig. 3, there is a decrease in the magnitude of the axial component of vorticity proportional to the increase in the longitudinal distance.

There are some discontinuities in the results presented in Fig. 3, which are likely caused by problems associated with an interpolation over relatively large axial distances. In spite of these shortcomings, this approach facilitates the analysis of the substructures' trajectories and the global characteristics in the axial component of vorticity. It is difficult to follow the trajectory of a substructure for a complete revolution around the vortex core because the substructures are either entrained into the vortex core or are dispersed as they approach the trailing edge of the wing. However, numerous half-rotations are evident in Fig. 3, which allow one to define the trace of helical trajectories. The trace of a helix is defined as $L/2\pi r$, where L is the longitudinal distance for one rotation and r is the radius of the helix. In Fig. 3 the substructures complete a half-rotation over a distance of 200–250 mm and have a radius of approximately 60 mm. Therefore the trace of the helix is between 0.53 and 0.66.

The ensemble of these three-dimensional LDV results confirms the formation and existence of corotating, stationary substructures in the separating shear layers, which form the leading-edge vortices. The evolution of the axial component of vorticity in the substructures and the helical path around the vortex core have been described. The current data do not permit a precise evaluation of the instability mechanism responsible for the creation of the substructures. However, the results do point toward the existence of convective instabilities near the leading edge. These detailed experimental results will provide a validation test case for future computational studies and analysis that might provide more precise flowfield details in the vicinity of the leading edge. These computational results are needed to confirm or disprove the many instability-related hypotheses presented in this Note. Additionally, computational results will provide further insight about the interaction of the substructures and the leading-edge vortex and the influence of the substructures on the vortex breakdown location.

Conclusions

The current data confirm the formation and existence of spatially stationary, corotating substructures in the shear layers that form the leading-edge vortices over slender delta wings at high angles of attack. The three-dimensional LDV data characterize the structure and path of these substructures around the leading-edge vortex cores, demonstrating their origin along the leading edges and their helical trajectories around the leading-edge vortices. However, the instability mechanism responsible for the creation of the substructures is still not well understood. Further research is required to explain the generating mechanism for the substructures and to examine the influence of these vortical substructures on the leading-edge vortex and the vortex breakdown location.

References

[1]Délery, J., "Physics of Vortical Flows," *Journal of Aircraft*, Vol. 29, No. 5, 1992, pp. 856–876.

[2]Werlé, H., "Sur l'Clatement des Tourbillons," ONERA, Note Technique 175, Meudon, France, Nov. 1971.

[3]Hall, M. G., "Vortex Breakdown," *Annual Review of Fluid Mechanics*, Vol. 4, 1972, pp. 195–218.

[4]Leibovich, S., "The Structure of Vortex Breakdown," *Annual Review of Fluid Mechanics*, Vol. 10, 1978, pp. 221–246.

[5]Sarpkaya, T., "On Stationary and Traveling Vortex Breakdowns," *Journal of Fluid Mechanics*, Vol. 45, Pt. 3, 1971, pp. 545–559.

[6]Nelson, R. C., "Unsteady Aerodynamics of Slender Wings," *Aircraft Dynamics at High Angles of Attack: Experiments and Modeling*, R-776, AGARD, 1991, pp. 1-1–1-26.

[7]Visbal, M. R., "Computational and Physical Aspects of Vortex Breakdown on Delta Wings," AIAA Paper 95-0585, Jan. 1995.

[8]Délery, J., "Aspects of Vortex Breakdown," *Progress in Aerospace Sciences*, Vol. 30, 1994, pp. 1–59.

[9]Gad-El-Hak, M., and Blackwelder, R. F., "The Discrete Vortices from a Delta Wing," *AIAA Journal*, Vol. 23, No. 6, 1985, pp. 961, 962.

[10]Reynolds, G., and Abtahi, A., "Three Dimensional Vortex Development, Breakdown and Control," AIAA Paper 89-0998, March 1989.

[11]Gordnier, R. E., "Computation of a Kelvin-Helmholtz Instability for Delta Wing Vortex Flows," Flight Dynamics Directorate, Wright Lab., WL-TR-91-3098, Wright–Patterson AFB, OH, Nov. 1991.

[12]Squire, H. B., Jones, J. G., and Stanbrook, A., "An Experimental Investigation of the Characteristics of Some Plane and Cambered 65 Deg Delta Wings at Mach Numbers from 0.7 to 2.0," Aeronautical Research Council, R&M 3305, London, 1961.

[13]Payne, F. M., Ng, T. T., Nelson, R. C., and Schiff, L. B., "Visualization and Wake Surveys of Vortical Flow over a Delta Wing," *AIAA Journal*, Vol. 26, No. 2, 1988, pp. 137–143.

[14]Lowson, M. V., "Visualization Measurements of Vortex Flows," AIAA Paper 89-0191, Jan. 1989.

[15]Verhaagen, N. G., Meeder, J. P., and Verhelst, J. M., "Boundary Layer Effects of the Flow of a Leading-Edge Vortex," AIAA Paper 93-3463, Aug. 1993.

[16]Washburn, A. E., and Visser, K. D., "Evolution of Vortical Structures in the Shear Layer of Delta Wings," AIAA Paper 94-2317, June 1994.

[17]Lowson, M. V., Riley, A. J., and Swales, C., "Flow Structure over Delta Wings," AIAA Paper 95-0586, Jan. 1995.

[18]Honkan, A., and Andreopoulos, J., "Instantaneous Three-Dimensional Vorticity Measurements in Vortical Flow over a Delta Wing," *AIAA Journal*, Vol. 35, No. 10, 1997, pp. 1612–1620.

[19]Ng, T. T., and Oliver, D. R., "Leading-Edge Vortex and Shear Layer Instabilities," AIAA Paper 98-0313, Jan. 1998.

[20]Drazin, P. G., and Reed, W. H., *Hydrodynamic Stability*, Cambridge Univ. Press, Cambridge, England, U.K., 1981.

[21]Ho, C. M., and Huerre, P., "Perturbed Free Shear Layer," *Annual Review of Fluid Mechanics*, Vol. 16, 1984, pp. 365–424.

[22]Molton, P., "Etude Experimentale de l'Clatement Tourbillonnaire sur aile Delta en Coulement Incompressible: Caracterisation du Champ Externe," ONERA, RT 53/1147AN, Meudon, France, 1992.

[23]Mitchell, A. M., "Caracterisation et Contr le de l'Clatement Tourbillonnaire sur une Aile Delta aux Hautes Incidences," Ph.D. Dissertation, Dept. de Mecanique, Univ. de Paris 6, Paris, July 2000.

[24]Mitchell, A. M., and Molton, P., "Vortical Substructures in the Shear Layers Forming Leading-Edge Vortices," AIAA Paper 2001-2424, June 2001.

[25]Barberis, D., "Test Cases for CFD Validation," ONERA, TP 1993-161, Meudon, France, 1993.

W. J. Devenport
Associate Editor